

Orbital ordering and magnetic structures in $\text{Sr}_{2-x}\text{La}_x\text{FeMoO}_6$ and $\text{Sr}_{2-x}\text{La}_x\text{FeWO}_6$ double perovskites.

A. Taraphder^{1,2}, and F. Guinea¹

¹ *Instituto de Ciencia de Materiales de Madrid, CSIC, Cantoblanco, E-28043 Madrid, Spain*

² *Department of Physics and Center for Theoretical Studies, Indian Institute of Technology, Kharagpur 721302, India*

We analyzed the possible magnetic and orbital orderings of double perovskites, using a simple extension of the double exchange model well suited for these compounds. Orbital ordering is favored by the on site repulsion at the Fe ions. We obtain a rich phase diagram, including ferri- and antiferromagnetic phases, which can, in turn, be metallic or insulating, depending on the existence of orbital order.

PACS numbers:

I. INTRODUCTION

Ferromagnetic double perovskites of composition $\text{Sr}_{2-x}\text{La}_x\text{FeMoO}_6$ (where La can be substituted by other double valency ions), known since some time¹ have attracted a great deal of attention recently, because of their high Curie temperature, metallic character, large magnetoresistance and potential applications^{2,3,4,5,6,7,8,9}. While lattice distortions and phonons do not seem to play a major role, disorder and in particular the antisite defects play a significant role in the properties of these compounds^{10,11,12,13,14,15,16,17}. Effects of doping have also been extensively studied^{18,19,20,21,22,23,24,25} recently. Related family of compounds based on Sr_2FeWO_6 are, on the other hand, insulating and antiferromagnetic^{26,27}. Solid solutions including Mo and W ions have also been studied^{28,29,30}.

The magnetic and electronic structures of the double perovskites with composition $\text{Sr}_{2-x}\text{La}_x\text{FeMoO}_6$ admit a simple description⁴. The Mo^{5+} and Fe^{3+} ions are located at the alternate nodes of a simple cubic lattice. The strong exchange coupling within the d orbitals of the Fe ion leads to the formation of a spin 5/2 moment, from electrons which occupy the exchange-split two \mathbf{e}_g and the three \mathbf{t}_{2g} orbitals. The three remaining three \mathbf{t}_{2g} orbitals at the Fe sites are hybridized, through the intermediate O ion, with the \mathbf{t}_{2g} orbitals of the neighboring Mo ions. Because of the symmetry of these orbitals, hopping between them can only take place along two of the three lattice axes, leading to three decoupled two dimensional bands. Band structure calculations suggest that the direct hopping between the Mo \mathbf{t}_{2g} orbitals is not negligible (this hopping does not change the two dimensional nature of the bands). The number of electrons in the conduction band, per unit cell, is $x = 1 + x$ where x is the concentration of the divalent La^{2+} ions. Most of the calculations reported below are given in terms of the band filling, x , and the correspondence with the doping level, x , is highlighted when needed.

These arguments suggest that the minimal description of the electronic structure of these materials requires three parameters: the energy difference between the \mathbf{t}_{2g}

levels in the Fe and Mo ions, $\Delta = \epsilon_{\text{Mo}} - \epsilon_{\text{Fe}}$, the Fe-Mo hopping, $t_{\text{Fe-Mo}}$, and the Mo-Mo hopping, $t_{\text{Mo-Mo}}$. We assume that the exchange splitting between the spin \mathbf{t}_{2g} states in the Fe ions is much larger than the width of the conduction band. Hence, we need to consider one spin state at each Fe ion. This truncation of the states used to describe the conduction band is similar to the one used in reducing the two band ferromagnetic Kondo lattice to the single band double exchange model, used in the study of $\text{La}_{1-x}\text{Ca}_x\text{MnO}_3$ and related compounds. This tight binding model can also be used to study the Sr_2FeWO_6 compound²⁷.

The phase diagram of the hybridized Mo-Fe system described above has been studied using the dynamical mean field method³¹, and within an exact treatment of the electronic wavefunction which allows for the study of defects³². Using realistic values for the parameters the Curie temperature is comparable to the one experimentally observed. The generic features of the phase diagram have some resemblance to those of double exchange model, to which it can be reduced in some limits. One of the most remarkable differences is the appearance of an antiferromagnetic phase even in the absence of direct antiferromagnetic interactions³².

The analysis outlined above implicitly assumes the equivalence of the three \mathbf{t}_{2g} orbitals at the Fe and Mo sites, and it neglects the possibility of non trivial types of orbital order. Electron electron interactions may break the symmetry between the \mathbf{t}_{2g} orbitals. Such phases have been extensively investigated in the related double exchange compounds of composition $\text{La}_{1-x}\text{Ca}_x\text{MnO}_3$ and related materials^{33,34,35,36,37,38,39}. The electron electron interaction in $\text{Sr}_{2-x}\text{La}_x\text{FeMoO}_6$ can be large, as the conduction band has a significant weight on the Fe orbitals. In the present paper, we analyze the possibility of the breaking of the orbital symmetry in the $\text{Sr}_{2-x}\text{La}_x\text{FeMoO}_6$ family of compounds, using mean field theory. The electron-electron interactions are described by means of a local repulsion term, U , between electrons in different orbitals at the same Fe site. Orbital ordering has already been reported for the stoichiometric Sr_2FeWO_6 compound²⁷. We obtain a rich phase diagram, as a function of the number of electrons in the

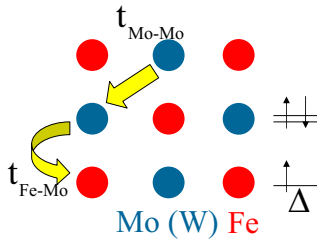


FIG. 1: (Color online). Sketch of the interactions included in \mathcal{H}_{kin} , eq.(1).

conduction band and the difference between the Fe and Mo levels. The method is discussed in the next section. Then, we present the main results. Section IV discusses the relevance of our findings for the physical properties of these materials.

II. THE MODEL AND THE METHOD OF CALCULATION.

We assume that the conduction band arises from the hybridization of t_{2g} orbitals at the Mo and Fe sites. There are three spin polarized orbitals at the Fe ion, and six orbitals at the Mo ion. The hopping takes place within planes determined by the symmetry of the orbitals (for instance, the hybridization does not allow for hopping between d_{xy} orbitals along the z axis). There is hopping only between states with the same spin. The levels at the Fe sites are shifted with respect to those at the Mo sites by an energy Δ . Within these approximations, the kinetic energy of the conduction electrons is described by three independent hamiltonians of the form:

$$\mathcal{H}_{\text{kin}}^{\alpha=1,2,3} = t_{\text{Fe-Mo}} \sum_{i,j,n.,s} c_{\alpha,i,s}^\dagger d_{\alpha,j,s} + t_{\text{Mo-Mo}} \sum_{ij,n.n.,s} c_{\alpha,i,s}^\dagger c_{\alpha,j,s} + \Delta_\alpha \sum_{i,s} d_{\alpha,i,s}^\dagger d_{\alpha,i,s} \quad (1)$$

The operators $c_{\alpha,i,s}$ create electrons with spin s in the orbital α at a Mo site, i , and the operators $d_{\alpha,i,s}^\dagger$ have the same effect at Fe sites. Note that the index s is either 1 or -1 at the Fe sites, while it can take both values at the Mo sites. We have conserved the spin index at the Fe sites in order to describe antiferromagnetic phases along (111) planes, like that observed in Sr_2FeWO_6 (see below). A schematic representation of the couplings in eq.(1) is shown in Fig.[1].

The hamiltonian \mathcal{H}_{kin} is defined on a square lattice. The resulting energy bands depend on the configuration of the core spins at the Fe sites. We will consider the two textures shown in Fig.[2]. When all core spins are parallel, the unit cell includes one Fe and one Mo site. The subbands with spins antiparallel to the core spins are built up from one orbital at the Fe site and another orbital at the Mo(W) site. The energies, $\epsilon_{\mathbf{k}}$, are given by:

$$\text{Det} \begin{vmatrix} 4t_{\text{Mo-Mo}} \cos(\mathbf{k}_x a) \cos(\mathbf{k}_y a) - \epsilon_{\mathbf{k}} & t_{\text{Fe-Mo}} e^{i\mathbf{k}_x a} e^{i\mathbf{k}_y a} \\ t_{\text{Fe-Mo}} e^{-i\mathbf{k}_x a} e^{-i\mathbf{k}_y a} & \Delta_\alpha - \epsilon_{\mathbf{k}} \end{vmatrix} = 0 \quad (2)$$

The band with spin parallel to the Fe core spins is localized at the Mo sites. The energy is:

$$\epsilon_{\mathbf{k}} = 4t_{\text{Mo-Mo}} \cos(\mathbf{k}_x a) \cos(\mathbf{k}_y a) \quad (3)$$

In the antiferromagnetic configuration shown in the right side of Fig.[2] the unit cell includes four sites. The spin

up and spin down bands are degenerate, although they are localized in different regions of the lattice. The spin up band is derived from two orbitals at the Mo sites, and the orbital at the Fe site whose core has spin down. The energies are given by:

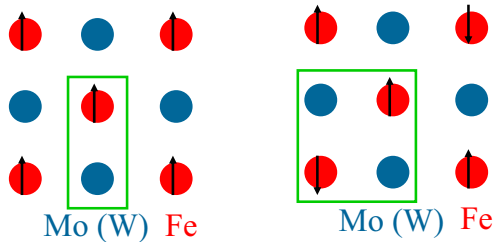


FIG. 2: (Color online). Configurations of the core spins at the Fe ions considered in the text. The rectangles denote the corresponding unit cell.

$$\text{Det} \begin{vmatrix} -\epsilon_{\mathbf{k}} & t_{\text{Mo-Mo}}(1 + e^{i\mathbf{k}_x a})(1 + e^{i\mathbf{k}_y a}) & t_{\text{Fe-Mo}}(1 + e^{-i\mathbf{k}_x a}) \\ t_{\text{Mo-Mo}}(1 + e^{-i\mathbf{k}_x a})(1 + e^{-i\mathbf{k}_y a}) & -\epsilon_{\mathbf{k}} & t_{\text{Fe-Mo}}(1 + e^{-i\mathbf{k}_y a}) \\ t_{\text{Fe-Mo}}(1 + e^{i\mathbf{k}_x a}) & t_{\text{Fe-Mo}}(1 + e^{i\mathbf{k}_y a}) & \Delta_{\alpha} - \epsilon_{\mathbf{k}} \end{vmatrix} = 0 \quad (4)$$

We also include a repulsion between electrons in different orbitals at the Fe sites. This term has the form:

$$\mathcal{H}_{\text{int}} = U \sum_{i, \alpha \neq \alpha'} d_{i, \alpha, s}^{\dagger} d_{i, \alpha, s} d_{i, \alpha', s}^{\dagger} d_{i, \alpha', s} \quad (5)$$

We use the Hartree-Fock method to analyze the effect of this term. Then, assuming that the occupancies of the different orbitals at the Fe site are not the same, the Fe levels are given by:

$$\Delta_{\alpha} = \epsilon_{\text{Fe}} - \epsilon_{\text{Mo}} + U \sum_{\alpha' \neq \alpha} \langle d_{i, \alpha', s}^{\dagger} d_{i, \alpha', s} \rangle \quad (6)$$

Here, ϵ_{Fe} and ϵ_{Mo} are defined in the absence of interaction corrections. The values of the expectation values $\langle d_{i, \alpha', s}^{\dagger} d_{i, \alpha', s} \rangle$ have to be calculated selfconsistently, inserting the levels given in eq.(6) into eq.(1).

Note that the filling of the conduction bands, x can vary between 0 and 9, $0 \leq x \leq 9$. In the following we will show calculations for band fillings within this range, although fillings such that $x \geq 2$ cannot be obtained by substituting the divalent Sr ions by trivalent ions.

From the total energy versus doping curves (see below) we identify regions of phase separation in the phase diagram using the Maxwell construction. This construction allows us to identify densities at which different phases can coexist as they have the same chemical potential.

III. RESULTS.

In the following, we use as unit of energy $t_{\text{Fe-Mo}}$. From band structure calculations⁴, this parameter is $t_{\text{Fe-Mo}} \approx 0.3\text{eV}$. We also fix $t_{\text{Mo-Mo}} = 0.2t_{\text{Fe-Mo}}$ and $U = 12t_{\text{Fe-Mo}}$. These values are less well defined, but consistent with existing band structure calculations⁴. The results do not change qualitatively for other values of these parameters, although the finer details are modified. We vary $\Delta = \epsilon_{\text{Fe}} - \epsilon_{\text{Mo}} + U/3$ from 0 (strongly hybridized band, probably adequate for $\text{Sr}_{2-x}\text{La}_x\text{FeMoO}_6$) to $\Delta = -4t_{\text{Fe-Mo}}$ (conduction electrons mostly localized on Fe ions, valid for $\text{Sr}_{2-x}\text{La}_x\text{FeWO}_6$). The filling of the conduction band can vary from 0 to 9. Experimentally relevant values of band filling (x) lie between 1 and 2, corresponding to doping levels, x , such that $0 \leq x \leq 1$.

Results for the total energy of selfconsistent solutions for $\Delta = -4t_{\text{Fe-Mo}}$ are shown in Fig.[3]. This case favors the localization of the conduction electrons at the Fe sites, a situation which probably describes well $\text{Sr}_{2-x}\text{La}_x\text{FeWO}_6$ ²⁷. The energy difference (per site) of the different phases is much smaller than the electronic kinetic energy. The most stable phase around $x = 0$ is the antiferromagnetic phase with orbital ordering. One of the three t_{2g} orbitals at the Fe site is occupied, while the two others are pushed to higher energies. This phase is insu-

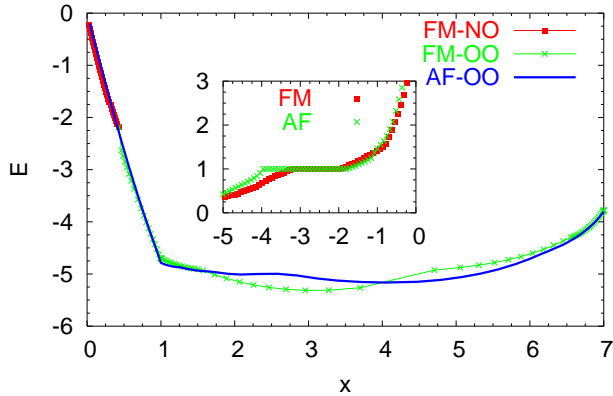


FIG. 3: (Color online). Total energy (per site) of the ferrimagnetic solutions with and without orbital ordering and for the antiferromagnetic solution (orbitally ordered) as a function of band filling, x . The splitting between the Fe and Mo levels is $\Delta = \epsilon_{\text{Fe}} - \epsilon_{\text{Mo}} + U/3 = -4t_{\text{Fe-Mo}}$. Inset: band filling (vertical axis) as function of chemical potential (horizontal axis) in units of $t_{\text{Fe-Mo}}$. Note that the doping is equal to the band filling minus one. OO stands for orbitally ordered, and NO for orbital degeneracy. FM and AF stand for the ferrimagnetic and antiferromagnetic phases discussed in the text.

lating, as shown in the kink of the energy vs. x curve, and the finite range of values of the chemical potential compatible with the band filling equal to one (doping $x = 0$), shown in the inset. This range gives the gap in the electronic spectrum, which is of order $1 - 2 \times t_{\text{Fe-Mo}}$. Our calculations suggest a wide range of phase coexistence, between the stoichiometric case, with doping $x = 0$, and doping $x \approx 1$. At sufficiently high dopings, an orbitally ordered ferrimagnetic phase is stable.

The nature of the insulating phase in this regime is in agreement with the band structure calculations in²⁷. One of the bands with spin antiparallel to the core Fe spin lies separated by a gap from the others. This band can accommodate one electron, and doping beyond $x = 0$ requires the filling of states above this gap.

The opposite case, where the Fe and Mo orbitals are optimally hybridized ($\Delta = 0$), is shown in Fig.[4]. This choice of parameters is probably adequate for $\text{Sr}_{2-x}\text{La}_x\text{FeMoO}_6$. The most stable phase near $x = 0$ is a metallic ferrimagnetic phase, without orbital ordering. At sufficiently high dopings, however, the antiferromagnetic, orbitally ordered phase prevails. These results are consistent with the calculations in³², although the antiferromagnetic phase is shifted towards larger values of x , due to the different value of $t_{\text{Mo-Mo}}$ used here. There is a first order phase transition between these two phases, with a significant range of doping values for which phase separation takes place. The two competing phases are metallic throughout the physically relevant doping range.

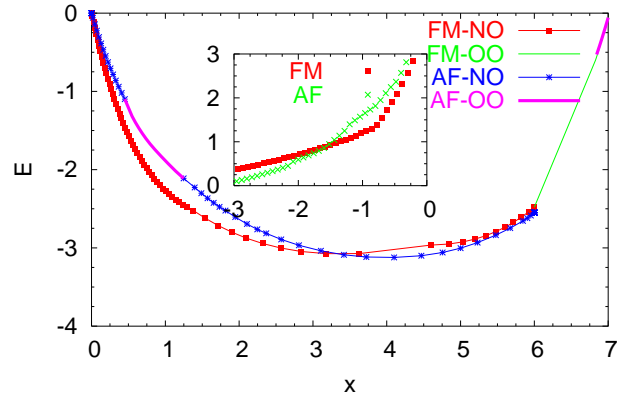


FIG. 4: (Color online). As in figure[3], but for $\Delta = 0$.

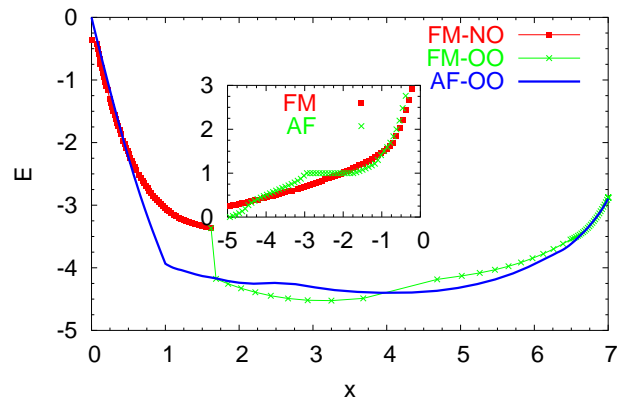


FIG. 5: (Color online). As in figure[3], but for $\Delta = -3t_{\text{Fe-Mo}}$.

The most complex intermediate situation between these two regimes takes place for $\Delta = -3t_{\text{Fe-Mo}}$, as shown in Fig.[5]. The orbitally ordered antiferromagnetic phase competes with the ferrimagnetic phase with and without orbital order. At low dopings, $x \leq 0$, the ferrimagnetic phase is the most stable. The insulating, orbitally ordered antiferromagnetic phase prevails near zero doping, $x = 0$, and the ferrimagnetic phase with orbital order has the lowest energy for $x \geq 0.6$. There are sizable regions of phase separation around $x = 0$.

The difference between the orbital levels at the Fe ion, which can be used to characterize the orbital order is shown in Fig.[6]. At low band fillings, when orbital order exists, the level splitting is, roughly, $\delta_1 - \delta_2 \approx Ux$. This effect leads, for $x = 1$ to a sizeable gap between the highest occupied and the lowest empty bands, as discussed above.

The phase diagram which arises from these calculations is shown in Fig.[7]. There is a competition between the different phases considered here, with regions of phase

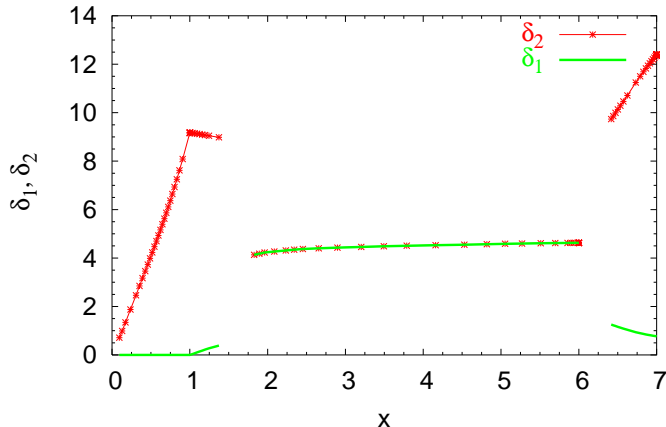


FIG. 6: (Color online). Splitting of the orbital levels at the Fe ions for $\Delta = -2t_{\text{Fe-Mo}}$ as function of band filling, x , in units of $t_{\text{Fe-Mo}}$.

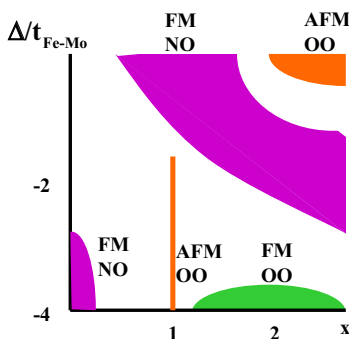


FIG. 7: (Color online). Schematic view of the phase diagram as function of the separation between the Fe and Mo(W) levels and the band filling x . FM and AF denote the ferrimagnetic and antiferromagnetic phases described in the text. OO stands for orbital order, and NO labels a phase without orbital order. The antiferromagnetic phase at $x = 1$ is insulating. Phase separation takes place in the blank regions.

separation.

IV. CONCLUSIONS.

We have studied the phase diagram of a tight binding model compatible with the known results about the band

structure of $\text{Sr}_{2-x}\text{La}_x\text{FeMoO}_6$ and $\text{Sr}_{2-x}\text{La}_x\text{FeWO}_6$. The model used resembles the double exchange model proposed for the manganites. The presence of a non magnetic ion (Mo,W) with levels at similar energies to the orbital levels of the magnetic ion (Fe) induces significant changes in the resulting magnetic structures. The large (threefold) degeneracy of the t_{2g} levels involved also influences the phase diagram.

The presence of non magnetic ion favors phases without net magnetization, if the band filling is such that the conduction electrons tend to reside in the non magnetic ion. This situation can be relevant for $\text{Sr}_{2-x}\text{La}_x\text{FeMoO}_6$ at sufficiently large dopings. At lower dopings (band filling $x \rightarrow 0$), and in a strongly hybridized band, the material tends to be a ferromagnetic metal, through a mechanism similar to double exchange.

Orbital order is favored when the conduction electrons are mostly localized in the magnetic, highly correlated ion (Fe). Then, a single band splits from the rest, leading to a system which is insulating at stoichiometry, $x = 0$ (band filling $x = 1$). This phase can be either ferrimagnetic or antiferromagnetic, with a slight tendency towards the latter. This situation may describe $\text{Sr}_{2-x}\text{La}_x\text{FeWO}_6$. We have not analyzed the suppression of orbital order at finite temperatures. The existence of a large gap in the insulating phase adequate for $\text{Sr}_{2-x}\text{La}_x\text{FeWO}_6$ implies that, within the Hartree Fock approximation, orbital order persists above the Néel temperature. This insulating phase is separated by regions of phase separation from other stable phases at different dopings. A similar situation arises in the single band Hubbard model at half filling⁴⁰.

The orbital ordering may be difficult to observe in a system which tends to be highly disordered, such as $\text{Sr}_{2-x}\text{La}_x\text{FeMoO}_6$ and $\text{Sr}_{2-x}\text{La}_x\text{FeWO}_6$. Orbital order favors anisotropic electronic properties, at each of the t_{2g} orbitals selects a plane perpendicular to one of the axes of the cubic lattice. The formation of domains because of antisites or other types of disorder can restore isotropy, although the system should be anisotropic at short length scales.

V. ACKNOWLEDGMENTS.

We are thankful to J. A. Alonso, L. Brey, L. A. Fernández, J. Fontcuberta, M. García-Hernández, V. Martín-Mayor and D. D. Sarma for many helpful conversations and comments during the course of this work. We are also thankful to Ministerio de Ciencia y Tecnología (Spain) for financial support through grant MAT2002-0495-C02-01. One of us (A. T.) is thankful to Ministerio de Educación y Cultura (Spain) for a sabbatical stay.

-
- ¹ A. Sleight and J. Weiher, *J. Phys. Chem. Solids* **33**, 679 (1972).
- ² K. I. Kobayashi, T. Kimura, H. Sawada, K. Terakura, and Y. Tokura, *Nature (London)* **395**, 677 (1998).
- ³ K. I. Kobayashi, T. Kimura, H. Sawada, K. Terakura, and Y. Tokura, *Phys. Rev. B* **59**, 11159 (1999).
- ⁴ D. D. Sarma, P. Mahadevan, T. Saha-Dasgupta, S. Ray, and A. Kumar, *Phys. Rev. Lett.* **85**, 2549 (2000).
- ⁵ J. Gopalakrishnan, A. Chattopadhyay, S. Ogale, T. Venkatesan, R. Greene, A. Millis, K. Ramesha, B. Hannoyer, and G. Marest, *Phys. Rev. B* **62**, 9538 (2000).
- ⁶ C. Ritter, M. R. Ibarra, L. Morellón, J. Blasco, J. García, and J. D. Teresa, *J. Phys.: Condens. Matter* **12**, 8295 (2000).
- ⁷ L. Balcells, J. Navarro, M. Bibes, A. Roig, B. Martínez, and J. Fontcuberta, *Appl. Phys. Lett.* **78**, 781 (2001).
- ⁸ M. Tovar, M. T. Causa, A. Butera, J. Navarro, B. Martínez, J. Fontcuberta, and M. C. G. Passeggi, *Phys. Rev. B* **66**, 024409 (2002).
- ⁹ M. Venkatesan, M. Grafoute, A. P. Douvalis, J.-M. Greneche, R. Suryanarayanan, and J. M. D. Coey, *J. Magn. Magn. Mater.* **242-245**, 744 (2002).
- ¹⁰ A. S. Ogale, S. B. Ogale, R. Ramesh, and T. Venkatesan, *Appl. Phys. Lett.* **75**, 537 (1999).
- ¹¹ D. D. Sarma, R. Nagarajan, S. Majumdar, A. Kumar, G. Nalini, and T. N. G. Row, *Solid State Commun.* **114**, 465 (2000).
- ¹² M. García-Hernández, J. Martínez, M. Martínez-Lope, M. Casais, and J. Alonso, *Phys. Rev. Lett.* **86**, 2443 (2001).
- ¹³ T. Saha-Dasgupta and D. Sarma, *Phys. Rev. B* **64**, 064408 (2001).
- ¹⁴ Y. Moritomo, N. Shimamoto, S. Xu, A. Machida, E. Nishibori, M. Takata, M. Sakata, and A. Nakamura, *Jpn. J. Appl. Phys.* **40**, L672 (2001).
- ¹⁵ J. M. Greneche, M. Venkatesan, R. Suryanarayanan, and J. M. D. Coey, *Phys. Rev. B* **63**, 174403 (2001).
- ¹⁶ D. Sánchez, J. A. Alonso, M. García-Hernández, M. J. Martínez-Lope, J. L. Martínez, and A. Mellergard, *Phys. Rev. B* **65**, 104426 (2002).
- ¹⁷ C. Frontera and J. Fontcuberta, *Phys. Rev. B* **69**, 014406 (2004).
- ¹⁸ Y. Moritomo, S. Xu, T. Akimoto, A. Machida, N. Hamada, K. Ohoyama, E. Nishibori, M. Takata, and M. Sakata, *Phys. Rev. B* **62**, 14224 (2000).
- ¹⁹ J. Navarro, C. Frontera, L. Balcells, B. Martínez, and J. Fontcuberta, *Phys. Rev. B* **64**, 092411 (2001).
- ²⁰ D. Serrate, J. M. D. Teresa, J. Blasco, M. R. Ibarra, and L. Morellón, *Appl. Phys. Lett.* **80**, 4573 (2002).
- ²¹ C. Frontera, D. Rubi, J. Navarro, J. L. García-Muñoz, J. Fontcuberta, and C. Ritter, *Phys. Rev. B* **68**, 115101 (2003).
- ²² C. Frontera, D. Rubi, J. Navarro, J. L. García-Muñoz, J. Fontcuberta, and C. Ritter, *Phys. Rev. B* **68**, 012412 (2003).
- ²³ M. Wojcik, E. Jedryka, S. Nadolski, J. Navarro, D. Rubi, and J. Fontcuberta, *Phys. Rev. B* **69**, 100407 (2004).
- ²⁴ M. Wojcik, E. Jedryka, S. Nadolski, D. Rubi, C. Frontera, J. Fontcuberta, B. Jurca, N. Dragoe, and P. Berthet (2004), cond-mat/0406161.
- ²⁵ J. Navarro, J. Fontcuberta, M. Izquierdo, J. Avila, and M. C. Asensio, *Phys. Rev. B* **69**, 115101 (2004).
- ²⁶ K. Kawanaka, I. Hase, S. Toyama, and Y. Nishihara, *J. Phys. Soc. Jap.* **68**, 2890 (1999).
- ²⁷ Z. Fang, K. Terakura, and J. Kanamori, *Phys. Rev. B* **63**, 180407 (2001).
- ²⁸ H. Linden, T. Yamamoto, J. Nakamura, M. Karppinen, and H. Yamauchi, *Appl. Phys. Lett.* **18**, 2736 (2001).
- ²⁹ Linden, T. Yamamoto, J. Nakamura, H. Yamauchi, and M. Karppinen, *Phys. Rev. B* **66**, 184408 (2002).
- ³⁰ A. P. Douvalis, M. Venkatesan, J. M. D. Coey, M. Grafoute, J. M. Greneche, and R. Suryanarayanan, *J. Phys. C: Condens. Matter* **14**, 12611 (2002).
- ³¹ K. Phillips, A. Chattopadhyay, and A. J. Millis, *Phys. Rev. B* **67**, 125119 (2003).
- ³² J. L. Alonso, L. A. Fernández, F. Guinea, F. Lesmes, and V. Martín-Mayor, *Phys. Rev. B* **67**, 214423 (2003).
- ³³ J. van den Brink, G. Khaliullin, and D. Khomskii, *Phys. Rev. Lett.* **83**, 5118 (1999).
- ³⁴ T. Hotta, A. Feiguin, and E. Dagotto, *Phys. Rev. Lett.* **86**, 4922 (2001).
- ³⁵ T. Maitra and A. Taraphder, *Europhys. Lett.* **59**, 896 (2002).
- ³⁶ T. Maitra and A. Taraphder, *Phys. Rev. B* **68**, 174416 (2003).
- ³⁷ T. Maitra and A. Taraphder, *Europhys. Lett.* **65**, 262 (2004).
- ³⁸ H. Aliaga, D. Magnoux, A. Moreo, D. Poilblanc, S. Yunoki, and E. Dagotto, *Phys. Rev. B* **68**, 104405 (2003).
- ³⁹ L. Brey, *Phys. Rev. Lett.* **92**, 127202 (2004).
- ⁴⁰ F. Guinea, E. Louis, M. P. López-Sancho, and J. A. Vergés, *Solid. St. Commun.* **113**, 593 (2000).